Metrol. Meas. Syst., Vol. 30 (2023) No. 4, pp. 773–790
DOI: 10.24425/mms.2023.147949

PAN POLSKA AKADEMIA NAUK

METROLOGY AND MEASUREMENT SYSTEMS
Index 330930, ISSN 0860-8229
www.metrology.wat.edu.pl

M&MS

STATOR-ROTOR FAULT DIAGNOSIS OF INDUCTION MOTOR BASED ON TIME-FREQUENCY DOMAIN FEATURE EXTRACTION

Lingzhi Yi[1,2], Jiao Long[1)], Yahui Wang[1)], Tao Sun[3)], Jianxiong Huang[1)], Yi Huang[1)]

1) College of Automation and Electronic Information, Xiangtan University, Xiangtan, Hunan, 411105, China (*ylzwyh@xtu.edu.cn, 1115693463@qq.com,* ✉ *wangyh1993@hnu.edu.cn, 1245988952@qq.com*)
2) Hunan Engineering Research Center of Multi-Energy Cooperative Control Technology, Xiangtan, Hunan 411105, China
3) State Grid Anhui Electric Power Ultra-High Voltage Company, Hefei, Anhui, 230000, China (*1543100483@qq.com*)

Abstract

Since the induction motor operates in a complex environment, making the stator and rotor of the motor susceptible to damage, which would have significant impact on the whole system, efficient diagnostic methods are necessary to minimize the risk of failure. However, traditional fault diagnosis methods have limited applicability and accuracy in diagnosing various types of stator and rotor faults. To address this issue, this paper proposes a stator-rotor fault diagnosis model based on time-frequency domain feature extraction and *Extreme Learning Machine* (ELM) optimized with *Golden Jackal Optimization* (GJO) to achieve high-precision diagnosis of motor faults. The proposed method first establishes a platform for acquiring induction motor stator-rotor fault data. Next, wavelet threshold denoising is used to pre-process the fault current signal data, followed by feature extraction to perform time-frequency domain eigenvalue analysis. By comparison, the impulse factor is finally adopted as the feature vector of the diagnostic model. Finally, an induction motor fault diagnosis model is constructed by using the GJO to optimize the ELM. The resulting simulations are carried out by comparing with neural networks, and the results show that the proposed GJO-ELM model has the highest diagnostic accuracy of 94.5%. This finding indicates that the proposed method outperforms traditional methods in feature learning and classification of induction motor fault diagnosis, and has certain engineering application value.

Keywords: Induction motor, time-frequency domain feature extraction, Golden Jackal Optimization, fault diagnosis.

1. Introduction

The motor drive system is an important electric energy equipment to support national economic development and national defence construction, as well as the key and core of major infrastructure [1–3]. Once the fault occurs in such a system, it can directly affect the normal operation of an electrical circuit and even cause serious safety accidents and economic losses.

Article history: received May 31, 2023; revised August 13, 2023; accepted August 19, 2023; available online November 16, 2023.

Through the monitoring of its running state, faults can be found and eliminated in time [4, 5]. This is why it is extremely important to perform accurate motor troubleshooting. Stator and rotor faults are the most common faults in motors. Carrying out stator and rotor fault diagnosis is of great significance for improving the reliability and safety of motor system operation [6].

Traditional fault diagnosis methods mostly rely on manual feature extraction of motor signals [7, 8]. During fault diagnosis, human factors interfere greatly, resulting in poor accuracy of diagnosis results and complex diagnosis process. Intelligent fault diagnosis technology exhibits glaring advantages over conventional fault detection techniques [9, 10]. Based on deep learning, building a fault diagnosis model by learning historical fault data has been widely concerned [11–13]. Shan *et al.* [14] extracted fault features from the response signals of the measurable points of the motor to be tested. Then a *back propagation neural network* (BPNN) was optimized using adaptive variational particle swarm algorithm to establish a transformer fault diagnosis model. This method improved the diagnostic accuracy, however, the high computational cost limited the application of deep learning model in fault diagnosis. Also, a lightweight multi-sensor fusion model for induction motor data fusion and diagnosis was proposed in the literature [15], introducing reverse residual blocks and network architecture search techniques. Compared with other popular neural networks, this method could accurately determine the fault category with a shorter prediction time. However, there were few learning samples, and the diagnostic accuracy needed to be improved. In response to the problem of insufficient samples for deep learning, many researchers have made sample expansion efforts [16, 17]. Shu *et al.* utilized a *Deep Convolutional Generative Adversarial Network* (DCGAN) to produce synthetic fault data and expand the training dataset [18]. However, despite its strong generalization and high recognition accuracy, generating simulation samples could lead to loss of critical features. Zhou *et al.* transformed the problem of diagnosing motor faults into identifying the parameters of the fault and achieving real-time detection [5]. Regrettably, this approach could only detect the presence of a fault in the motor, and not classify its type. Xue *et al.* proposed a *Fuzzy Operation Safety Assessment* (FOSA) system [19]. The system employed several symptom parameters to represent electrical and mechanical faults from various perspectives, using the theory of possibility to obtain membership functions as the assessment model. However, due to the significant level of subjective bias, the model cold suffer from inaccuracies.

There are many signals that can be used to detect motor faults such as vibration signals, stator current signals, *etc.* Lee, Jong-Hyun proposed a fault diagnosis system for induction motor using a *Convolutional Neural Network* (CNN) model that utilized vibration signals [20]. In the literature [21], an automatic fault diagnosis system based on *Residual Neural Network 101* (ResNet101) is proposed, which unifies pre-processing and state sensing of motor fault signals under one framework to achieve end-to-end intelligent fault diagnosis. However, motors typically operate under non-stationary conditions, which make fault diagnosis significantly challenging due to the highly complex nature of the vibration signals. In addition, noise interference affects the effectiveness of feature extraction. Also, a stator-rotor fault detection method based on the stator current signal has the advantages of low price and non-invasiveness, and is widely studied and applied. Li W *et al.* [22] illustrated that the use of stator current signals to detect stator-rotor faults is superior to vibration signals. In contrast, vibration signals are more suitable for detecting bearing faults in motors. Fault diagnosis methods based on stator current signal methods combined with machine learning have recently received a lot of attention. A method for intelligent fault diagnosis using a residual network optimized initiation - Intelligent Industrial Fault Diagnosis using Sailfish Optimized Inception with Residual Network (IIFD-SOIR) model has been proposed in the literature [23]. The proposed model operates on three main processes: signal extraction, feature extraction and classification. In the literature [24], a novel fault diagnosis

method combining CNN and ELM is proposed based on the current signal. However, the two methods above are limited to setting of network parameters.

To address the problems above, a stator-rotor fault diagnosis model for induction motors is proposed based on time-frequency domain feature extraction and GJO-ELM to achieve high-precision diagnosis of motor faults. The paper's primary contributions are:

1. An induction motor stator and rotor fault data collection platform is built. By replacing the motor model, the faulty motor under different conditions is simulated. Then the current data of three types of stator and rotor faults: stator winding fault, bent rotor shaft, and broken rotor strip are collected.
2. Through pre-processing and eigenvalue analysis in the time-frequency domain, the fault feature vector-pulse factor which can accurately represent the monitored induction motor is extracted.
3. The parameters of the extreme learning machine are optimized by using the GJO algorithm, and the fault diagnosis model of the induction motor with the highest accuracy is built to realize the high-precision fault diagnosis of the induction motor.

The layout of this paper is as follows: First, the purpose of this work is explained in Section 1. The theoretical approaches to data denoising and time-frequency domain analysis are introduced in Section 2 together with the data acquisition system. In Section 3, the construction of the GJO-ELM-based induction motor stator-rotor fault detection model is described. Section 4 provides the experiments and an analysis of the findings. Section 5 offers the conclusions.

2. Signal data acquisition and time-frequency domain analysis

A reliable and sufficient data set is the key to improve the accuracy of fault diagnosis models. In this paper, we propose building a data acquisition system to collect a large amount of current signal data of different fault types. As induction motors are inevitably disturbed by noise during operation, the current signal data needs to be pre-processed by denoising so that the signal data retains the characteristics of the original signal data [25]. Time-frequency domain analysis is performed to obtain the eigenvalues and subsequently perform induction motor fault diagnosis.

2.1. Data acquisition system of induction motor fault

In order to verify the effectiveness of induction motor stator-rotor fault diagnosis, it is first necessary to collect current signal data for different fault types. Therefore, a power dragging system as shown in Fig. 1 can be used for fault experiments on induction motors. During the experiment, the two-phase stator currents are sampled through a current clamp, connected to an oscilloscope that can generate data. By replacing the motor model, different faulty motors are simulated to complete the current acquisition experiment under multiple faults. In this paper, the current signals of three types of stator-rotor faults $i.e.$ stator winding fault, rotor bending, and rotor broken strip are collected as the total sample for the experiment. The sampling frequency is 400Hz, and the time of each sampling is set to 5 seconds, so the data collected for each group of signals is 2000 each time. The current data collected consists of 500 groups containing 2000 consecutive sampling points for each type of state, containing 3–4 cycles of current signals, as the total sample for the experiment. The oscilloscope can save the current waveform to the PC, and the file type selected by us for this purpose is CSV. The selected time and numerical data are imported into the MATLAB workspace, and the fault diagnosis model can be trained and tested.

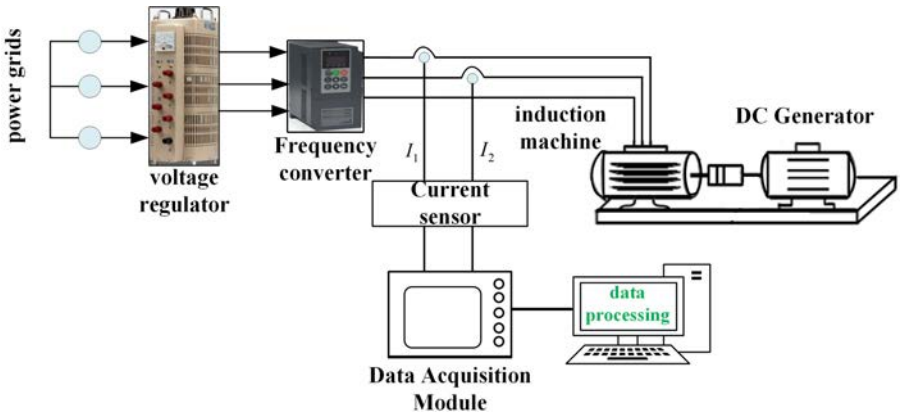

Fig. 1. Induction motor data acquisition system.

Stator winding failures are caused by moisture or vibration leading to wear, resulting in the insulation layer of the winding being rubbed. The resistance of the insulation is reduced. This, in turn, leads to a *i.e.*, short circuit. The fault process has the electrical characteristics of a sudden change in resistance value. Therefore, in this paper the stator winding fault is simulated by connecting a resistor to one phase of the stator winding. Bending of the shaft can occur when the motor is not used for a long time, too fast speed, improper maintenance, impact, excessive load and thermal expansion caused by temperature. In this case, the centre of the rotor does not coincide with the axis of rotation, so in this paper we simulate the shaft bending fault by bending the centre of the rotor. A broken rotor bar occurs when the motor is frequently started or is overloaded during operation. The long-term effect is of such use is that potentially dangerous phenomena are triggered such as rotor fracture or open welding. In serious cases, the motor will be burned out, which constitutes a potential accident risk. In this paper, the rotor breakage fault is tested with a broken rotor installed instead of an operational one.

The experimental induction motor system relies on a symmetric, three-phase power supply for energy. To regulate the voltage and frequency of the motor, a voltage regulator and frequency converter are utilized. The experimental motor is a 1.5 kW induction motor and the load is a 1.8 kW DC generator. The two motors are connected through an elastic coupling, and the load can also be connected with a variable resistor. The experimental motor is a YSP90L-4 induction motor. Its main parameters are shown in Table 1. The samples of different types of faults were collected as shown in Table 2.

Table 1. Induction motor experimental parameters.

Model	YSP90L-4		
Rated power (kW)	1.5	**Rated speed (r/min)**	1400
Nominal voltage (V)	380	**Polar logarithm**	2
Rated frequency (Hz)	50	**Wiring method**	Y
Power Factor	0.79	**Ambient temperature(^{o}C)**	40
Efficiency	88.5%	**Insulation grade**	B

Metrol. Meas. Syst., Vol. 30 (2023), No. 4, pp. 773–790
DOI: 10.24425/mms.2023.147949

Table 2. Fault samples collected.

Motor state	Description	Number of samples
Stator winding turn-to-turn short circuit	A resistor connected to one phase of the stator winding	(500, 2000)
Bending of the rotor shaft	Spindle centre bent	(500, 2000)
Rotor broken bar	Rotor breakage	(500, 2000)

2.2. Wavelet thresholding denoising

The effectiveness of the fault diagnosis model mainly depends on the effectiveness of the extracted feature quantity and the selection of the classifier. There is a certain noise signal in the original current signal, which will interfere with the diagnosis results. Therefore, a denoising process is needed first. The principle of wavelet denoising is that when decomposing signal data and noise interference data, signal data and noise will be decomposed according to different eigenvalues. And the characteristics of the original signal data can be preserved to a great extent, so that the preserved signal data is true and feasible [26]. Figure 2 depicts the wavelet threshold denoising flowchart. Mode maxima denoising, wavelet correlation coefficient denoising, and wavelet threshold denoising are the three primary fundamental techniques for wavelet denoising. This section focuses on wavelet-based threshold denoising for data pre-processing.

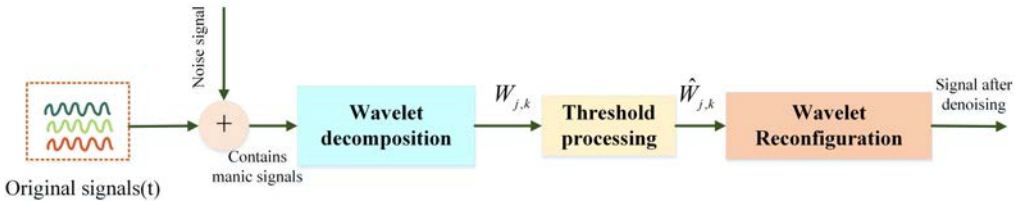

Fig. 2. Wavelet threshold denoising flow chart of induction motor detection signal.

There is a difference in the wavelet coefficient amplitude between the signal data and the noise data. The corresponding wavelet coefficients of the two are also different and will show negative correlation characteristics, thus realizing the processing of wavelet threshold denoising. Different threshold selection in wavelet threshold denoising has different effects on noise processing. There are three main thresholds applied here and these are: the hard threshold, the soft threshold and the fixed threshold. A garrote function is used for fixed thresholds. The hard threshold is shown in (1) and the soft threshold is shown in (2), where is the wavelet coefficient and is the threshold value:

$$\hat{w}_{j.k} = \begin{cases} w_{j.k} & w_{j.k} \geq \lambda \\ 0 & w_{j.k} < \lambda \end{cases}, \tag{1}$$

$$\hat{w}_{j.k} = \begin{cases} \operatorname{sgn}(w_{j.k}) \left(|w_{j.k}| - \lambda\right) & w_{j.k} \geq \lambda \\ 0 & w_{j.k} < \lambda \end{cases}. \tag{2}$$

The *signal-to-noise ratio* (SNR) represents the ratio of energy between signal and noise (see (3)). The root *mean square error* (RMSE) explains the degree of dispersion between the two

signals and also responds to the distortion of the signal. It is shown in (4):

$$\mathrm{SNR} = 10\lg\left(\frac{p_s}{p_n}\right) = 10\lg\left(\frac{\sum_{t=1}^{N} f^2(t)}{\sum_{t=1}^{N}[f(t)-\hat{f}(t)]^2}\right), \tag{3}$$

$$\mathrm{RMSE} = \sqrt{\frac{1}{N}\sum_{j=1}^{N}[f(t)-\hat{f}(t)]^2}, \tag{4}$$

here is the power of the original signal; is noise power; N is the signal length; denotes the original signal and denotes the noise cancelling signal.

The larger the signal-to-noise ratio, the more noise is removed from the signal. The denoising effect is relatively ideal. The root-mean-square error is the opposite of the signal-to-noise ratio. The larger the value of the root mean square error, the larger the constant deviation between the two signals, and the worse the denoising effect. Therefore, the SNR and the RMSE of the estimated signal and the original signal can be used to judge the denoising effect.

2.3. Time and frequency domain analysis

The denoised signal is analysed in the time and frequency domains. The eigenvalues in the time domain are mean value, RMS, peak value, variance, standard deviation, peak factor, impulse factor, margin factor, *etc*. The eigenvalues in the frequency domain are mean frequency, root mean square frequency, centre frequency, variance frequency, *etc*. The formulas for the main time-frequency domain features are shown in Table 3. The time domain eigenvalues mainly

Table 3. Formulas for the main time-frequency domain features.

Mean value	$\bar{X} = \frac{1}{N}\sum_{i=1}^{n} x_i$	RMS	$X_{\mathrm{RMS}} = \sqrt{\frac{1}{N}\sum_{i=1}^{n} x_i^2}$
Peak value	$X_{p-p} = \max(x_i) - \min(x_i)$	Variance	$X_{\delta^2} = \frac{1}{N}\sum_{i=1}^{n}(x_i - \bar{x})^2$
Standard deviation	$X_{\mathrm{SD}} = \sqrt{x_{\delta}^2}$	Pulse factor	$C_{\mathrm{if}} = \frac{X_{\mathrm{peak}}}{\frac{1}{N}\sum_{i=1}^{n} x_i}$
Peak factor	$C = \frac{X_{\mathrm{peak}}}{\sqrt{\frac{1}{N}\sum_{i=1}^{n} x_i^2}}$	Margin factor	$C_{\mathrm{mf}} = \frac{X_{\mathrm{peak}}}{\left(\frac{1}{N}\sum_{i=1}^{n} \lvert x_i \rvert^{\frac{1}{2}}\right)^2}$
Centre frequency	$X_1 = \frac{\sum_{i=1}^{N_{\mathrm{ft}}} s_i s(i)}{\sum_{i=1}^{N_{\mathrm{ff}}} s(i)}$	Variance frequency	$X_2 = \sqrt{\frac{\sum_{i=1}^{N_{\mathrm{ff}}} (f_i - X_1)^2 s(i)}{\sum_{i=1}^{N_{\mathrm{ff}}} s(i)}}$

represent the relationship between the dynamic signal in terms of the time axis as a coordinate. The frequency domain eigenvalues mainly describe the frequency structure of the signal and the relationship between the frequency and the amplitude of the signal at that frequency.

3. Fault diagnosis model of the stator and rotor of an induction motor based on GJO-ELM

In the training process of the network model, the optimization goal has always been to predict the deviation between the classification results and the real category labels. The GJO algorithm is used to obtain the optimal fitness value by constantly adjusting the parameters of ELM, so as to get the optimal parameters of ELM, and then train and learn to obtain the fault diagnosis model with the highest diagnosis rate. This not only saves the time and workload of repeatedly adjusting the ELM hyperparameter but, at the same time, it ensures the good diagnostic accuracy and robustness of the fault diagnosis model.

3.1. GJO optimization algorithm

A metaheuristic optimization method called the Golden Jackal Optimization algorithm is adopted [27]. By imitating the cooperative hunting behaviour of the Golden Jackal, cooperation and information sharing among individuals in the group are achieved to find the optimal solution. Compared with other optimization algorithms, GJO well avoids getting trapped in local optimum. Its global optimization capability is stronger and the speed of finding the optimal solution is faster.

The GJO algorithm includes two basic steps: searching for prey, surrounding and attacking prey. They correspond to the exploration and exploitation of the population, respectively. The male jackal has the best fitness value, and the female jackal has the second-best fitness value. Jackal pairs obtain corresponding the position of the corresponding prey.

3.2. ELM

ELM is a single hidden layer feedforward neural network. It has the advantages of simple calculation, strong applicability and high efficiency. The ELM network structure is shown in Fig. 3. Its input weights w_{i1}, w_{i2} and w_{i3} are randomly generated in the ELM itself. It does not need iterative solution, but only needs to solve the weights from the hidden layer to the output layer. Therefore, compared with deep learning such as offered by a BP network, the training speed is greatly improved.

The ELM learning objective function x can be represented by the matrix as:

$$F(x) = \sum_{i=1}^{n} \beta_i \cdot \eta \left(w_i \cdot x_1 + b_i \right) = L, \tag{5}$$

where β_i is the weight of the hidden layer to the output layer; w_i is the weight of the hidden layer to the input layer; b_i is the bias of the hidden layer; η is the connection weight of the ith hidden layer node to the output node; n is the number of hidden points; and L is the desired output.

The network training is turned into a linear system to solve the problem, and β is determined according to $\beta = H^* \cdot L$ where H^* is the generalized inverse matrix of H. The stability of the neural network is enhanced by introducing the regularization coefficient C and the unit matrix I, which makes the matrix characteristic roots non-zero. As a result, the stability and generalization

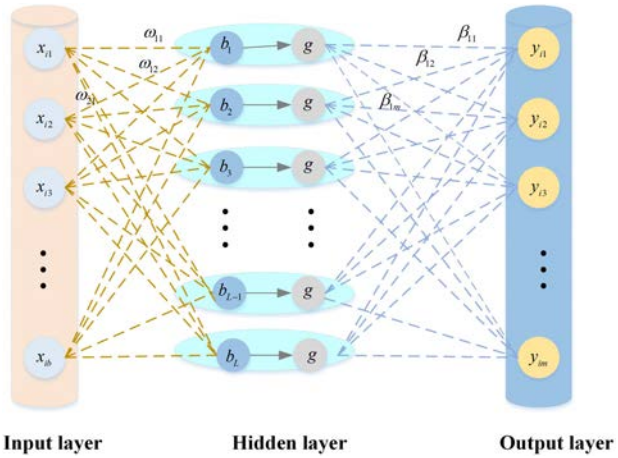

Fig. 3. Structure diagram of the ELM network.

are also better. The least squares solution of the output weight is:

$$\beta = H^T \left(HH^T + \frac{I}{C} \right)^{-1} L, \tag{6}$$

where β is the output weight vector connecting the implicit layer and the output layer; H is the feature mapping matrix.

3.3. Construction of the GJO-ELM fault diagnosis model

In this paper, the induction motor stator-rotor fault data acquisition platform is employed to collect current signals from various fault types. Wavelet threshold denoising is used for the pre-processing of the current signals. Time-frequency domain eigenvalue analysis determines the pulse factor as the eigenvector of the diagnostic model, which is then input to the GJO-ELM fault diagnosis model to enhance the diagnostic accuracy.

In this paper, the *Root Mean Square Error* (RMSE) of the classification model is chosen as the fitness function to be minimized by the optimization algorithm, which measures the deviation between predicted values and actual values.

$$\mathrm{RMSE}(X, f) = \sqrt{\frac{1}{n} \sum_{j=1}^{n} (f(x_i) - y_i)^2}, \tag{7}$$

where $f(x)$ is the predicted result and y is the true result.

The flow chart of the GJO-ELM induction motor stator-rotor fault intelligent diagnosis based on GJO-ELM is shown in Fig. 4. The GJO algorithm is used to synchronize the two parameters of the input weight w and the deviation b of the hidden node of the ELM to jointly find the optimum. Thus, the GJO-ELM model with the optimal fault diagnosis results is obtained.

The specific steps are as follows:

Step 1: Set the initial parameters. Initialize ELM related parameters. Initialize the relevant parameters of GJO optimization algorithm: set population size (pop), dimension (dim), maximum iteration times (Itermax), upper bound (u_b) and lower bound (l_b).

Step 2: Population initialization. The position of the initial Golden Jackal population is obtained.

Step 3: For each position after initialization, two parameters w, b of ELM are assigned. The fitness value of each individual Golden Leopard is calculated in turn. The ranking is performed and the position with the best fitness is recorded.

Step 4: The evasion energy E of the prey and the random number rl based on the Lévy distribution are calculated. When $|E| \geq 1$, the exploration phase is entered and the positions of male and female jackals at that time are calculated separately. Then update the position of the jackal after the next iteration. At the end of the exploration phase, the fitness value of each prey is calculated. If the fitness value is lower than the optimal position, the candidate position of that individual will replace the optimal position.

Step 5: When $|E| < 1$, the exploitation phase is entered and the positions of the male and female jackals are calculated separately at that time. Then the position of the jackals after the next iteration is updated. At the end of the exploitation phase, a population operation is performed. In this operation, the fitness values of all prey are calculated. A population position update is performed, and the best of the fitness values is used as the male jackal and the second best of the fitness values is used as the female jackal.

Step 6: The maximum iteration number is checked, and if fulfilled, the optimal parameters are assigned to the ELM. Conversely, if this condition is not met, return to Step 4 to continue iterating.

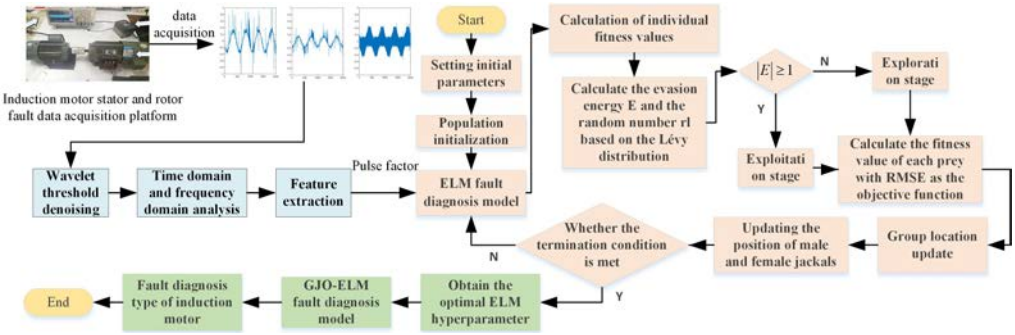

Fig. 4. Flow chart of intelligent diagnosis of stator and rotor faults in a GJO-ELM based induction motor.

4. Experiments and results analysis

4.1. Data pre-processing

The experimental motor is a YSP90L-4 induction motor. Its main parameters are shown in Table 1. The physical diagram of the induction motor data acquisition system is shown in Fig. 5. The oscilloscope can save current waveform data to PC, and the file type selected by us is CSV. By importing the selected time and numerical data into the MATLAB workspace, the data can be pre-processed and the fault diagnosis model can be trained and tested. Figure 6 shows a set of sampled waveforms of the A-phase stator current signal under different faults of the induction motor. They are stator winding an inter-turn short circuit, a rotor shaft bending, and a rotor broken strip fault, respectively.

In the process of wavelet threshold denoising, the selection of wavelet basis and decomposition levels, the selection criteria of threshold aa well as the design of the threshold function will have

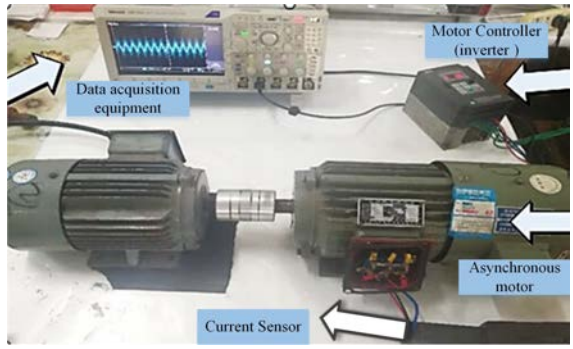

Fig. 5. Physical diagram of the induction motor data acquisition system.

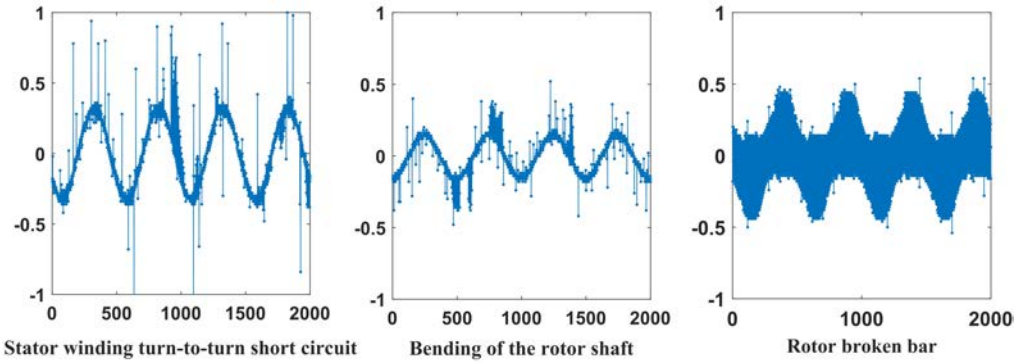

Fig. 6. Sampling waveform of A-phase stator current signal under different states of induction motor.

great influence on the final signal denoising effect. The Ym8 wavelet basis function has compact support and good continuity, and symmetry. Therefore, this paper uses the ym8 wavelet basis function to denoise the continuous and symmetrical stator current signal. After the signal is decomposed with the wavelet with scale 4, the coefficients of each layer are the thresholds. It can not only ensure that the signal is not distorted, but also achieve a good denoising effect. The results of denoising with different thresholds for stator winding inter-turn short circuit, rotor shaft bending, and rotor broken bar faults are shown in Figs 7, 8, 9.

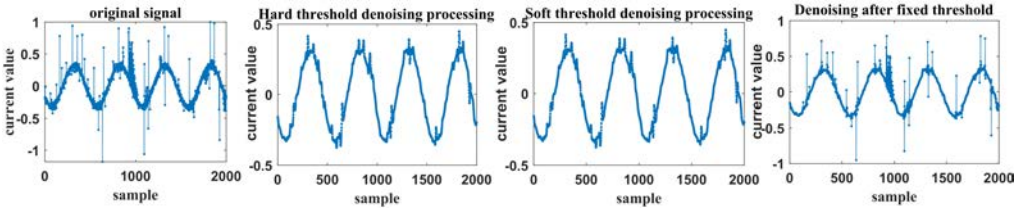

Fig. 7. Stator winding turn-to-turn short circuit fault.

The wavelet denoising effect of the stator winding inter-turn short circuit at different thresholds is shown in Table 4. The wavelet fixed threshold denoising method with the largest SNR and the

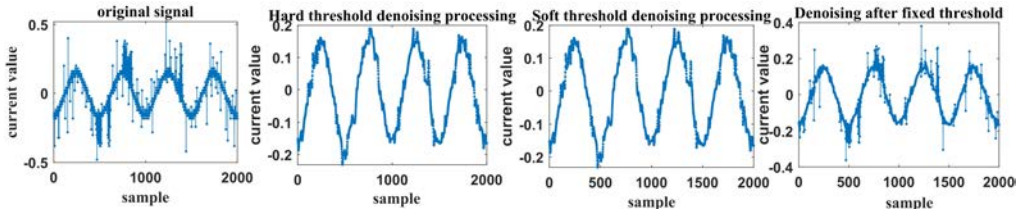

Fig. 8. Bending fault of the rotating shaft.

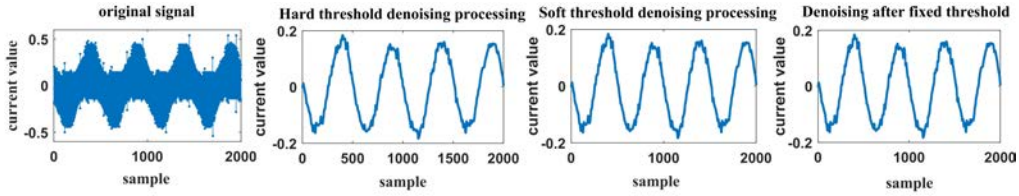

Fig. 9. Rotor broken bar failure.

smallest RMSE is selected. In addition, experiments show that the fixed threshold approach has the best effects in the case of shaft bending and rotor bar breaking faults. Therefore, the data after wavelet fixed threshold denoising is derived and feature extraction is carried out.

Table 4. Wavelet denoising effect of stator winding inter-turn short circuit at different thresholds.

Evaluation Indicators	Hard Threshold	Soft Threshold	Fixed Threshold
SNR	8.9261	8.9297	14.3168
RMSE	0.088689	0.088653	0.04768

4.2. Feature Extraction

The process of feature selection aims to remove irrelevant details while improving accuracy [27]. It is a crucial step because the performance of fault diagnosis methods heavily depends on the ability of the chosen features to precisely represent the fault characteristics of the monitored induction motor. The feature values of different stator-rotor faults after extraction of denoising are then analysed in the time and frequency domains. Next, the differences in the features of the different faults are analysed. The intelligent algorithm of machine learning is used to train the classification and then determine the different fault types to achieve the diagnosis of stator-rotor faults in induction motors.

The time domain and frequency domain eigenvalues for different faults after feature extraction are shown in Tables 5, 6 and 7.

From the time-domain and frequency-domain eigenvalues in Tables 5–7, it can be seen that the peak factor, pulse factor, margin factor and central frequency eigenvalues of the stator winding fault, the shaft bending fault and the rotor bar breaking fault are obviously different. In order to better select the feature values, this section focuses on extracting the features from them by repeating the experiments. The peak factor, pulse factor, margin factor and centre frequency of the

Table 5. Time domain eigenvalues for different fault types.

Fault location	Rectification average	Variance	Standard deviation	Cliff factor	Skewness
Stator winding fault	0.2143	0.0614	0.2479	2.8416	0.1144
Bending of the rotor shaft	0.1035	0.0151	0.1227	2.8999	0.0173
Rotor broken bar	0.2078	0.0584	0.2416	2.1636	0.0137

Table 6. Time domain eigenvalues for different fault types.

Fault location	Root mean square value	Waveform factor	Peak factor	Pulse factor	Margin factor	Peak value
Stator winding fault	0.2478	1.1566	8.7959	10.1731	11.4091	2.18
Bending of the rotor shaft	0.1228	1.1866	8.1453	9.5656	11.1730	1.68
Rotor broken bar	0.2416	1.1626	4.4709	5.1981	5.7270	1.28

Table 7. Frequency domain eigenvalues for different fault types.

Fault location	Mean frequency	Root mean square frequency	Centre frequency	Standard deviation frequency	Variance frequency
Stator winding fault	0.0037	0.2399	–0.0131	0.000231	0.001525
Bending of the rotor shaft	0.0020	0.1267	–0.0199	0.0000563	0.001325
Rotor broken bar	0.0019	0.2314	–0.0411	0.000148	0.001455

five experiments are shown in Figs 10, 11, 12 and 13, respectively. The maximum and minimum values of each type of fault characteristic value are marked with data cursors in the figures.

Observing the variation of the eigenvalues of each fault, it can be found that the peak factor, margin factor and centre frequency of both the stator winding fault and the rotor bending fault have intersecting parts. Therefore, these three eigenvalues cannot represent the characteristics of these two faults. As can be seen in Fig. 11, the pulse factor for stator winding faults is between

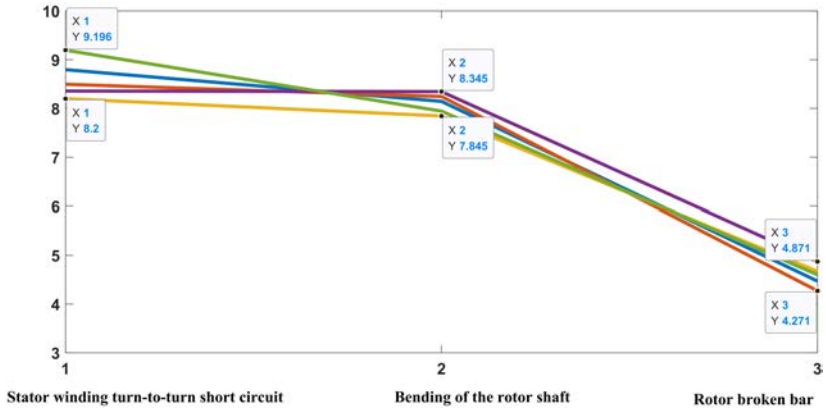

Fig. 10. Peak factor of stator and rotor faults in the five experiments.

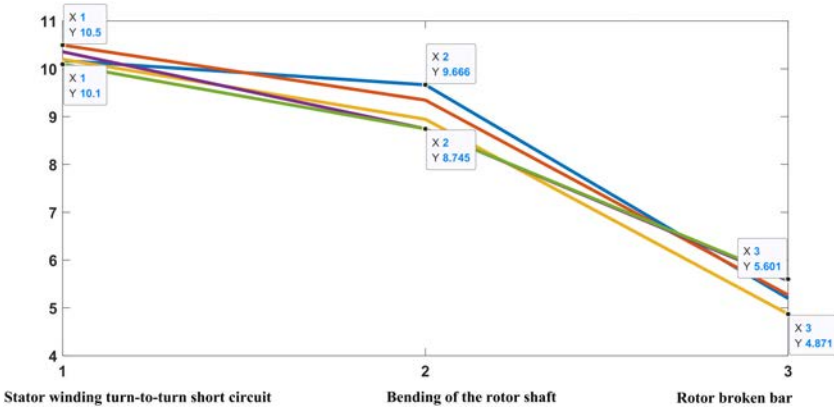

Fig. 11. Pulse factors of stator and rotor faults in the five experiments.

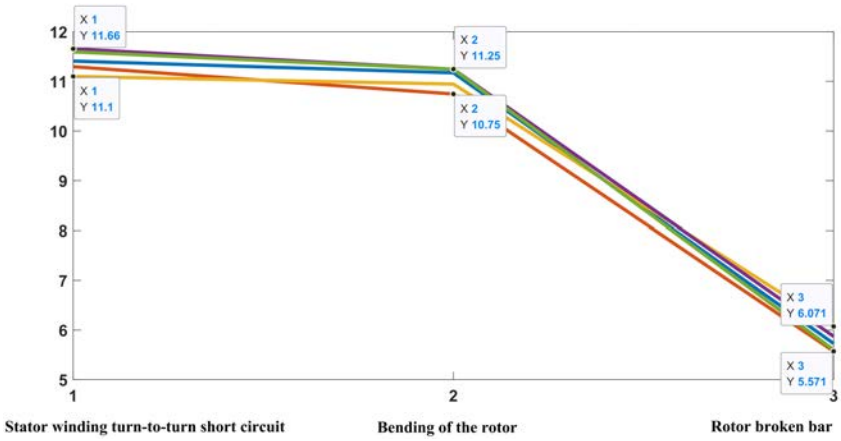

Fig. 12. Margin factor for five experimental stator-rotor failures.

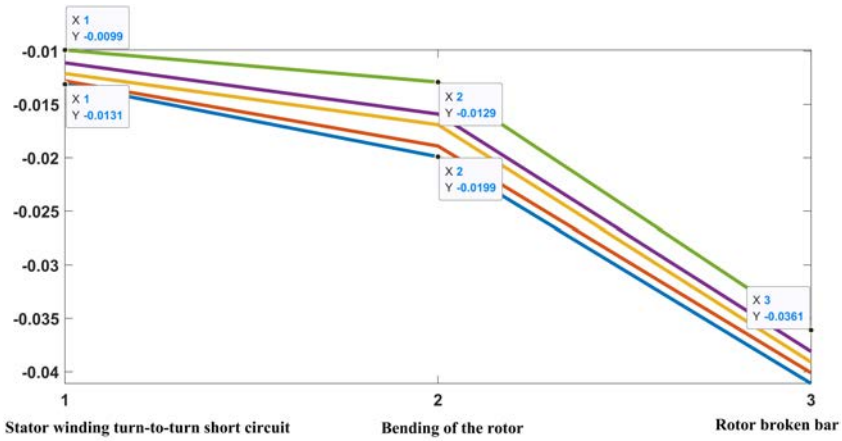

Fig. 13. Centre frequency of five experimental stator-rotor failures.

10–11, for rotor bending faults between 9–9.6, and for rotor broken bar faults between 4–6. Therefore, the pulse factor can be used to represent the features of these three faults. Through the analysis above, the value of the pulse factor is chosen to represent the features of stator-rotor faults in different parts.

4.3. Comparison analysis

In this section, for the three pre-processed fault current samples, 600 samples are randomly taken from each class to synthesize a new sample. It is then divided into a training set and a test set according to 8:2. The training set is fed into the model for learning. Labelling is performed according to the characteristics of faults with stator winding faults, bent rotor shafts and broken rotor bars. The average value of the pulse factor is used as the labelling of the faults. Since the input weight w and the deviation b of the hidden nodes in ELM are randomly generated, it affects the recognition accuracy of ELM. Therefore, the positions of male and female golden jackals of the updated GJO algorithm are used to adjust the input weights and hidden biases of ELM. Thus, the generalization ability and calculation speed of ELM are improved. Four diagnosis models of stator and rotor faults of induction motors, GJO-ELM, GJO-BPNN, ELM and BPNN, are constructed and compared. The intelligent diagnosis model of stator and rotor faults of an induction motor is trained by training samples. Then, the test set is used to test the diagnosis effect of each fault diagnosis model. The experimental results are shown in Figs 14, 15, 16 and 17. The diagnostic accuracy of different stator and rotor fault types is shown in Table 8.

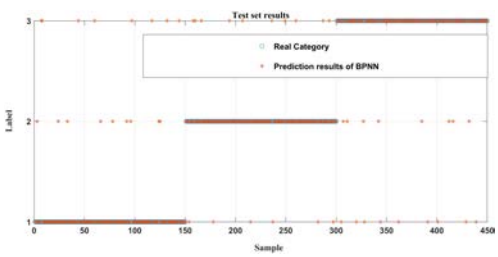

Fig. 14. BPNN test results graph.

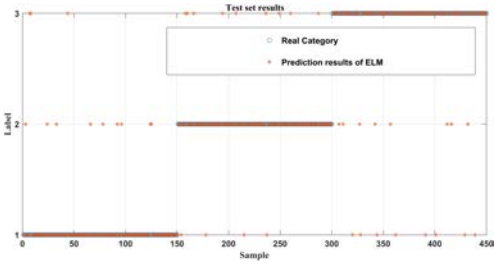

Fig. 15. ELM test results graph.

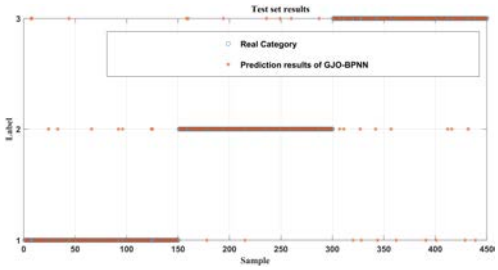

Fig. 16. GJO-BPNN test results graph.

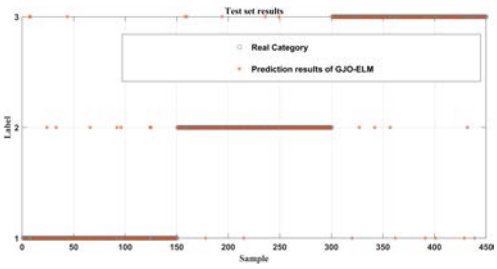

Fig. 17. GJO-ELM test results graph.

Through comparative analysis of Figs 14, 15, 16, and 17, it is evident that the accuracy of the GJO-ELM fault diagnosis model is the highest, reaching 94.5%. In contrast, the accuracy of the GJO-BPNN, ELM, and BPNN induction motor stator-rotor fault models are 92.3%, 90%, and 88.8%, respectively. This indicates that the diagnostic performance of the GJO-ELM fault

diagnosis model is significantly superior to that of the other models. Furthermore, when compared to the BPNN fault diagnosis model, the accuracy of the ELM fault diagnosis model is improved by approximately 2%, demonstrating the superiority of ELM. When compared to the ELM fault diagnosis model, the GJO-ELM fault diagnosis model is in accuracy improved by approximately 4%. This confirms the effectiveness and superiority of the GJO algorithm for optimization. The experiments validate that the proposed GJO-ELM model has robust fault classification capabilities. This model has high reliability and effectiveness when applied to the diagnosis of induction motor stator-rotor faults.

Table 8. Classification of different fault types by each model.

Fault Type Algorithm	**Stator winding fault**	**Bending of the rotor shaft**	**Rotor broken bar**
BPNN	88.67%	89.32%	88.61%
ELM	92.18%	91.37%	89.25%
GJO-BPNN	93.33%	94.00%	89.40%
GJO-ELM	**94.03%**	**96.12%**	**93.33%**

5. Conclusions

In this paper, the fault diagnosis of induction motor stator and rotor is performed by using an data acquisition platform, wavelet threshold denoising, time-frequency domain eigenvalue analysis and a GJO-ELM fault diagnosis model. The following conclusions are drawn:

1. Based on the data acquisition platform of stator and rotor faults of induction motor, the motor model is changed and the current acquisition experiments of different fault types are completed. The experimental results verify the reliability and accuracy of the data acquisition platform.
2. Using wavelet threshold denoising to pre-process the fault current signal data can retain the original information well. And the intrinsic connection of the sequence data is fully considered.
3. By means of time-frequency domain eigenvalue analysis, the use of the pulse factor can accurately represent the fault characteristics of the monitored induction motor. It improves the ability to distinguish between various feature vectors and solves the problem of difficult feature extraction. The pulse factor is used as the feature vector of the diagnosis model, which improves the diagnosis accuracy.
4. The GJO algorithm is used to optimize the superior parameters of the ELM, which saves the time and workload of repeatedly adjusting the ELM super parameters. The proposed GJO-ELM model has the highest diagnostic accuracy reaching 94.5%.

Acknowledgements

This work was supported by the National Natural Science Foundation of China (61572416), Hunan Province Natural Science Zhuzhou United Foundation (2022JJ50132), and the Postgraduate Scientific Research Innovation Project of the Hunan Province (QL20210153).

References

[1] Shi, S., Sun, Y., Li, X., Dan, H., & Su, M. (2020). Moving Integration Filter-Based Open-Switch Fault-Diagnosis Method for Three-Phase Induction Motor Drive Systems. *IEEE Transactions on Transportation Electrification*, *6*(3), 1093–1103. https://doi.org/10.1109/tte.2020.2999692

[2] Zeng, C., Huang, S., Lei, J., Wan, Z., & Yang, Y. (2021). Online Rotor Fault Diagnosis of Permanent Magnet Synchronous Motors Based on Stator Tooth Flux. *IEEE Transactions on Industry Applications*, *57*(3), 2366–2377. https://doi.org/10.1109/tia.2021.3058541

[3] Xu, C., Li, J., & Cheng, X. (2022). Comprehensive Learning Particle Swarm Optimized Fuzzy Petri Net for Motor-Bearing Fault Diagnosis. *Machines*, *10*(11), 1022. https://doi.org/10.3390/machines10111022

[4] Im, S.-H., & Gu, B.-G. (2022). Study of Induction Motor Inter-Turn Fault Part II: Online Model-Based Fault Diagnosis Method. *Energies*, *15*(3), 977. https://doi.org/10.3390/machines10111022

[5] Zhou, H., Liu, Z., & Yang, X. (2018). Motor Torque Fault Diagnosis for Four Wheel Independent Motor-Drive Vehicle Based on Unscented Kalman Filter. *IEE Transactions on Vehicular Technology*, *67*(3), 1969–1976. https://doi.org/10.1109/tvt.2017.2751750

[6] Sabouri, M., Ojaghi, M., Faiz, J., & Marques Cardoso, A. J. (2020). Model-based unified technique for identifying severities of stator inter-turn and rotor broken bar faults in SCIMs. *IET Electric Power Applications*, *14*(2), 204–211. https://doi.org/10.1049/iet-epa.2019.0267

[7] Lakehal, A. (2020). Bayesian graphical model based optimal decision-making for fault diagnosis of critical induction motors in industrial applications. *Bulletin of the Polish Academy of Sciences – Technical Sciences*, *68*(3), 467–476. https://doi.org/10.24425/bpasts.2020.133374

[8] Deng, F., Zhang, Z., Zhong, H., Zeng, X., Huang, Y., Zeng, Z., & Feng, S. (2023). Single-end traveling wave protection method in flexible DC transmission line based on dominant frequency attenuation characteristics. *International Journal of Electrical Power & Energy Systems, 152*, 109220. https://doi.org/10.1016/j.ijepes.2023.109220

[9] Wu, X., Zhang, Y., Cheng, C., & Peng, Z. (2021). A hybrid classification autoencoder for semi-supervised fault diagnosis in rotating machinery. *Mechanical Systems and Signal Processing*, *149*, 107327. https://doi.org/10.1016/j.ymssp.2020.107327

[10] Kabul, A., & Unsal, A. (2022). Diagnosis ff Multiple Faults of on Induction Motor Based on HilBert Envelope Analysis. *Metrology and Measurement Systems*, *29*(1), 191–205. https://doi.org/10.24425/mms.2022.138541

[11] Gljuscic, M., Franulovic, M., Lanc, D., & Bozic, Z. (2022). Application of digital image correlation in behavior modelling of AM CFRTP composites. *Engineering Failure Analysis*, *136*, 106133. https://doi.org/10.1016/j.engfailanal.2022.106133

[12] Wang, R., Feng, Z., Huang, S., Fang, X., & Wang, J. (2020). Research on Voltage Waveform Fault Detection of Miniature Vibration Motor Based on Improved WP-LSTM. *Micromachines*, *11*(8), 753. https://doi.org/10.3390/mi11080753

[13] Zhao, H., Liu, J., Chen, H., Chen, J., Li, Y., Xu, J., & Deng, W. (2022). Intelligent Diagnosis Using Continuous Wavelet Transform and Gauss Convolutional Deep Belief Network. *IEEE Transactions on Reliability*. https://doi.org/10.1109/tr.2022.3180273

[14] Shan, Y. (2022). Application of PSO Improved Algorithm in Motor Fault Diagnosis Simulation. *Wireless Communications & Mobile Computing*, 2022, 2386523 https://doi.org/10.1155/2022/2386523

[15] Wang, J., Fu, P., Ji, S., Li, Y., & Gao, R. X. (2022). A Light Weight Multisensory Fusion Model for Induction Motor Fault Diagnosis. *IEEE-ASME Transactions on Mechatronics*, *27*(6), 4932–4941. https://doi.org/10.1109/tmech.2022.3169143

[16] Zhang, D., Ning, Z., Yang, B., Wang, T., & Ma, Y. (2022). Fault diagnosis of permanent magnet motor based on DCGAN-RCCNN. *Energy Reports*, *8*, 616–626. https://doi.org/10.1016/j.egyr.2022.01.226

[17] Shao, S., Wang, P., & Yan, R. (2019). Generative adversarial networks for data augmentation in machine fault diagnosis. *Computers in Industry*, *106*, 85–93. https://doi.org/10.1016/j.compind.2019.01.001

[18] Shu, X., Yang, H., Zhou, H., Wei, K., Guo, Y., & He, S. (2021). Fault diagnosis and failure analysis of motor controller by the approach of Bayesian inference. *International Journal of Vehicle Design*, 86(1–4), 52–70. https://doi.org/10.1504/ijvd.2021.122251

[19] Xue, H., Ding, D., Zhang, Z., Wu, M., & Wang, H. (2022). A Fuzzy System of Operation Safety Assessment Using Multimodel Linkage and Multistage Collaboration for In-Wheel Motor. *IEEE Transactions on Fuzzy Systems*, *30*(4), 999–1013. https://doi.org/10.1109/tfuzz.2021.3052092

[20] Lee, J.-H., Pack, J.-H., & Lee, I.-S. (2019). Fault Diagnosis of Induction Motor Using Convolutional Neural Network. *Applied Sciences*, *9*(15), 2950. https://doi.org/10.3390/app9152950

[21] Shifat, T. A., & Hur, J.-W. (2021). ANN Assisted Multi Sensor Information Fusion for BLDC Motor Fault Diagnosis. IEEE Access, *9*, 9429–9441. https://doi.org/10.1109/access.2021.3050243

[22] Li, W. D., & Mechefske, C. K. (2006). Detection of induction motor faults: A comparison of stator current, vibration and acoustic methods. *Journal of Vibration and Control*, *12*(2), 165–188. https://doi.org/10.1177/1077546306062097

[23] Surendran, R., Khalaf, O. I., & Romero, C. A. T. (2022). Deep Learning Based Intelligent Industrial Fault Diagnosis Model. *Computers Materials & Continua*, *70*(3), 6323–6338. https://doi.org/10.32604/cmc.2022.021716

[24] Chen, Z., Gryllias, K., & Li, W. (2019). Mechanical fault diagnosis using Convolutional Neural Networks and Extreme Learning Machine. *Mechanical Systems and Signal Processing*, *133*, 106272. hrefhttps://doi.org/10.1016/j.ymssp.2019.106272https://doi.org/10.1016/j.ymssp.2019.106272

[25] Ali, M. Z., & Liang, X. (2020). Threshold-Based Induction Motors Single- and Multifaults Diagnosis Using Discrete Wavelet Transform and Measured Stator Current Signal. *Canadian Journal of Electrical and Computer Engineering – Revue Canadienne de Génie Electrique et Informatique*, *43*(3), 136–145. https://doi.org/10.1109/cjece.2020.2966114

[26] Chen, Q., Jiang, Y.,Tang, Y., Zhang, X., &Wang, C.(2022). An induction motor fault diagnosis method based on the time-frequency image method and an improved graph convolutioal network. *Journal of Vibration and Shock*, *41*(24), 241–248. https://doi.org/10.13465/j.cnki.jvs.2022.24.030

[27] Chopra, N., & Ansari, M. M. (2022). Golden ackal optimization: A novel nature-inspired optimizer for engineering applications. Expert Systems with Applications, *198*, 116924. https://doi.org/10.1016/j.eswa.2022.116924

[28] Fu, H., Sun, G., Ren, J., Zhang, A., & Jia, X. (2022). Fusion of PCA and Segmented-PCA Domain Multiscale 2-D-SSA for Effective Spectral-Spatial Feature Extraction and Data Classification in Hyperspectral Imagery. IEEE Transactions on Geoscience and Remote Sensing, *60*, 5500214. https://doi.org/10.1109/tgrs.2020.3034656

Lingzhi Yi obtained her M.Sc. and Ph.D. degrees respectively in 1999 and 2016 from Xiangtan University. She is currently a full professor (Level II) at the College of Automation and Electronic Information, Xiangtan University. Her research interests include power electronics, renewable energy and intelligent microgrid, *etc*.

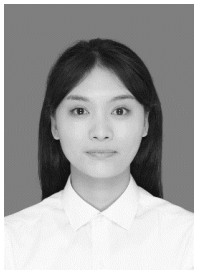

Jiao Long received her B.Sc. degree in Electronic Science and Technology from Hunan Institute of Engineering in 2021. She is currently working toward her M.Sc. degree at Xiangtan University, Xiangtan. Her interests include the research on intelligent algorithm and intelligent fault diagnosis.

Yahui Wang received her B.Sc. degree from the College of Electrical and Information Engineering, Hunan University, Changsha, China, in 2016. Then, she took a successive postgraduate and doctoral program in Electrical Engineering at Hunan University from 2016 to 2023. Currently, she is working at the College of Automation and Electronic Information, Xiangtan University. Her research interests include the optimization of smart grid, integrated multi-energy systems, and demand-side management.

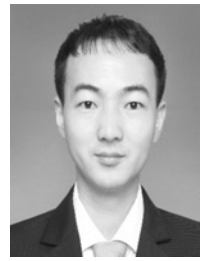

Tao Sun received his B.Sc. degree in Electric Engineering from West Anhui University, Lu'an, in 2020 and his M.Sc. degree from the College of Xiangtan University, Xiangtan, in 2023. He is currently working for the State Grid Anhui Electric Power Ultra-High Voltage Company, Hefei. His interests include the research on sliding mode control, intelligent algorithms and fault detection.

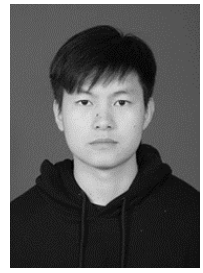

Jianxiong Huang received his B.Sc. degree in Electronic Message from Xi ' an Shiyou University in 2021. He is currently working toward his M.Sc. degree at Xiangtan University, Xiangtan. His interests include research on edge computing.

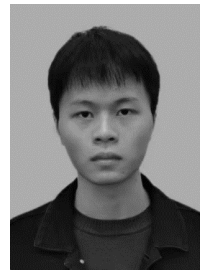

Yi Huang received his B.Sc. degree in Electric Engineering from Hunan Institute of Technology, in 2022. He is currently working toward the M.Sc. degree at Xiangtan University, Xiangtan. His interests include the research on sliding mode control, intelligent algorithms and fault detection.